

# High-Voltage Phosphate Cathodes for Rechargeable Ca-Ion Batteries

Sanghyeon Kim, Liang Yin, Myeong Hwan Lee, Prakash Parajuli, Lauren Blanc, Timothy T. Fister, Haesun Park, Bob Jin Kwon, Brian J. Ingram, Peter Zapol, Robert F. Klie, Kisuk Kang, Linda F. Nazar,\* Saul H. Lapidus, and John T. Vaughey\*



Cite This: *ACS Energy Lett.* 2020, 5, 3203–3211



Read Online

ACCESS |



Metrics & More

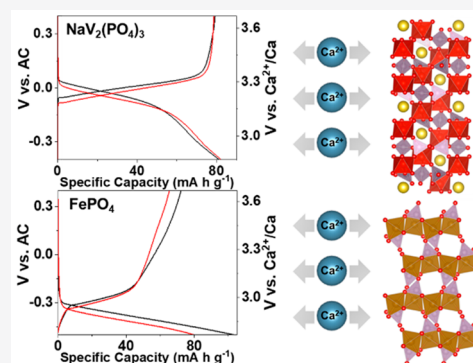


Article Recommendations



Supporting Information

**ABSTRACT:** Calcium-ion batteries (CIBs) are under investigation as next-generation energy storage devices due to their theoretically high operating potentials and lower costs tied to the high natural abundance of calcium. However, the development of CIBs has been limited by the lack of available positive electrode materials. Here, for the first time, we report two functional polyanionic phosphate materials as high-voltage cathodes for CIBs at room temperature.  $\text{NaV}_2(\text{PO}_4)_3$  electrodes were found to reversibly intercalate 0.6 mol of  $\text{Ca}^{2+}$  ( $81 \text{ mA h g}^{-1}$ ) near 3.2 V (vs  $\text{Ca}^{2+}/\text{Ca}$ ) with stable cycling performance at a current density of  $3.5 \text{ mA g}^{-1}$ . The olivine framework material  $\text{FePO}_4$  reversibly intercalates 0.2 mol of  $\text{Ca}^{2+}$  ( $72 \text{ mA h g}^{-1}$ ) near 2.9 V (vs  $\text{Ca}^{2+}/\text{Ca}$ ) at a current density of  $7.5 \text{ mA g}^{-1}$  in the first cycle. Structural, electronic, and compositional changes are consistent with reversible  $\text{Ca}^{2+}$  intercalation into these two materials.



For nearly 30 years, energy storage systems based on lithium-ion intercalation have been the energy storage system of choice for numerous applications ranging from portable electronics to electric vehicles because of their high energy density and good cycle life.<sup>1,2</sup> However, the identification of new research pathways that may allow LIB technology to reach higher energy densities is limited, creating an opportunity for alternative cation-based chemistries that may overcome these limits.<sup>3–5</sup> Among these beyond-lithium chemistries, energy storage concepts based on multivalent ions have received considerable attention as alternatives to LIBs, because theoretically, they have higher energy densities than LIBs when used in conjunction with metal anodes, as they have similar cell voltages, and the multivalent transporting cation may yield higher capacities.<sup>3–5</sup> Among the many multivalent battery systems ( $\text{Al}^{3+}$ ,  $\text{Ca}^{2+}$ ,  $\text{Mg}^{2+}$ ,  $\text{Zn}^{2+}$ ) being considered, calcium-ion batteries (CIB) appear to be particularly promising, as they provide the highest operating voltage among the multivalent systems due to the low  $\text{Ca}^{2+}/\text{Ca}$  reduction potential ( $-2.87 \text{ V}$  vs a standard hydrogen electrode).<sup>6,7</sup> Furthermore, as Ca salts are generally nontoxic, abundant, and widely available, new systems may have cost and recycling benefits. However, the development of CIBs has remained in a nascent stage due to the lack of functional electrode materials and effective electrolytes that enable efficient calcium plating and stripping. This is highlighted by recent advances in calcium metal electrodeposition that

represent a major step forward in the understanding of CIB anodes.<sup>8–15</sup> For continued CIB development, the discovery of high-voltage calcium-ion cathode materials would be a major step toward improving our understanding and creating new insights to further the field of CIBs. Efforts to develop CIB cathodes have been made mainly based on established intercalation materials such as Prussian blue analogues<sup>16–20</sup> and layered materials ( $\text{VOPO}_4 \cdot 2\text{H}_2\text{O}$ ,<sup>21</sup>  $\text{Mg}_{0.25}\text{V}_2\text{O}_5 \cdot \text{H}_2\text{O}$ ,<sup>22</sup>  $\text{MoO}_3$ ,<sup>23,24</sup>  $\text{V}_2\text{O}_5$ ,<sup>25</sup>  $\text{Ca}_{0.5}\text{CoO}_2$ <sup>26</sup>). Although these early works helped establish the needed materials design principles for future CIB studies, further improvements are necessary. For instance, Prussian blue analogues are difficult to dehydrate and often have issues with salt cointercalation, leading to low volumetric energy density.<sup>27</sup> Several layered oxide materials show significant capacitive behavior with large voltage hysteresis and without clear voltage plateaus during cycling probably due to a large overpotential.

The search for potential cathode insertion materials has been hampered by the relatively large ionic size of  $\text{Ca}^{2+}$  (e.g.,

Received: August 3, 2020

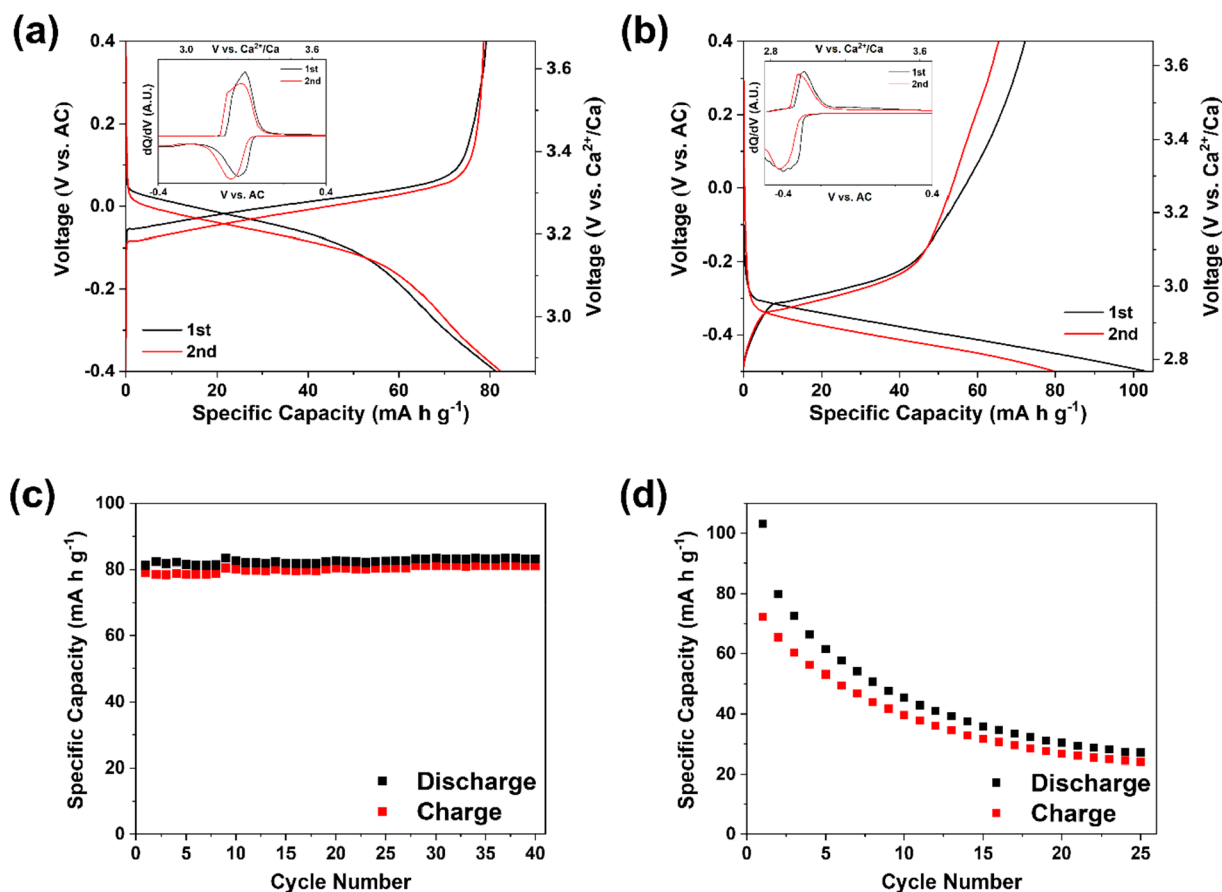
Accepted: September 14, 2020

Published: September 14, 2020



Table 1. Refined Unit Cell Dimensions<sup>a</sup> for Na<sub>3</sub>V<sub>2</sub>(PO<sub>4</sub>)<sub>3</sub> and LiFePO<sub>4</sub> at Different States of Charge

charge state	phase	<i>a</i> (Å)	<i>b</i> (Å)	<i>c</i> (Å)	$\alpha$ (deg)	$\beta$ (deg)	$\gamma$ (deg)	<i>V</i> (Å <sup>3</sup> )	space group
pristine	Na <sub>3</sub> V <sub>2</sub> (PO <sub>4</sub> ) <sub>3</sub>	15.11409 (5)	8.73032(3)	8.82809(3)	90	124.539(2)	90	959.5549(7)	<i>C2/c</i>
Na charged	NaV <sub>2</sub> (PO <sub>4</sub> ) <sub>3</sub>	8.42933(3)	8.42933(3)	21.4895(1)	90	90	120	1322.342(1)	<i>R<math>\bar{3}c</math></i>
Ca charged	NaV <sub>2</sub> (PO <sub>4</sub> ) <sub>3</sub>	8.42917(3)	8.42917(3)	21.4884(1)	90	90	120	1322.227(1)	<i>R<math>\bar{3}c</math></i>
pristine	LiFePO <sub>4</sub>	10.32411(3)	6.00591(2)	4.6934(2)	90	90	90	291.019(2)	<i>Pnma</i>
Li charged	FePO <sub>4</sub>	9.82534(8)	5.79554(4)	4.78388(4)	90	90	90	272.4092(4)	<i>Pnma</i>
Ca charged	FePO <sub>4</sub>	9.81763(8)	5.79273(4)	4.7836(4)	90	90	90	272.0475(4)	<i>Pnma</i>

<sup>a</sup>Rietveld refinements to synchrotron data.Figure 1. First and second cycle galvanostatic discharge–charge curves of (a) NaV<sub>2</sub>(PO<sub>4</sub>)<sub>3</sub> at 3.5 mA g<sup>-1</sup> and (b) FePO<sub>4</sub> at 7.5 mA g<sup>-1</sup> at room temperature. The insets show the corresponding differential capacity plots. Cycling performance of (c) NaV<sub>2</sub>(PO<sub>4</sub>)<sub>3</sub> at 3.5 mA g<sup>-1</sup> and (d) FePO<sub>4</sub> at 7.5 mA g<sup>-1</sup> at room temperature.

Ca<sup>2+</sup>: 114 pm, Na<sup>+</sup>: 116 pm, Li<sup>+</sup>: 90 pm), which limits its ability to fit into several common ionically conductive framework structures (i.e., spinel), the complex interfacial chemistry of multivalent cations, and the high activation energy barrier originating from the divalent charge of Ca<sup>2+</sup> ions.<sup>6,7,28</sup> In this light, three-dimensional (3D) structures built on redox active transition metals and polyanions (XO<sub>4</sub>)<sub>n</sub><sup>-</sup> (X: P, Si, S), are promising candidates for Ca-ion battery electrodes. Such highly covalent three-dimensional frameworks can generate large stable interstitial spaces capable of supporting calcium insertion and extraction.<sup>29–33</sup> Higher cell voltages can also be achieved with the introduction of polyanion groups that increase the redox potential by the inductive effect.<sup>29–31</sup>

Here, we demonstrate two representative polyanion phosphates as new high-voltage CIB cathodes. NaV<sub>2</sub>(PO<sub>4</sub>)<sub>3</sub> and FePO<sub>4</sub> were chosen, as they are electrochemically active with sodium cations (Na<sup>+</sup> (116 pm), which has a similar ionic

radius to Ca<sup>2+</sup> (114 pm)) and other studied multivalent intercalation cations (Zn<sup>2+</sup>, Mg<sup>2+</sup>, Al<sup>3+</sup>).<sup>34–41</sup> In our study, we observed reversible calcium intercalation at high voltage at room temperature in a nonaqueous electrolyte. Importantly, we utilized numerous multiple characterization techniques, including synchrotron XRD, XAS, EELS, and EDS analysis to elucidate and confirm reversible calcium intercalation.

The polyanionic host materials, NaV<sub>2</sub>(PO<sub>4</sub>)<sub>3</sub> and FePO<sub>4</sub>, were prepared by the electrochemical oxidation of Na<sub>3</sub>V<sub>2</sub>(PO<sub>4</sub>)<sub>3</sub> and LiFePO<sub>4</sub>, respectively. Vacant lattice sites for Ca<sup>2+</sup> intercalation were created, via electrochemical removal of Na<sup>+</sup> and Li<sup>+</sup> from Na<sub>3</sub>V<sub>2</sub>(PO<sub>4</sub>)<sub>3</sub> and LiFePO<sub>4</sub>, respectively (Figures S1a and S2a). Specifically, Na<sub>3</sub>V<sub>2</sub>(PO<sub>4</sub>)<sub>3</sub> was charged at 5 mA g<sup>-1</sup> up to 0.5 V vs activated carbon (AC), and LiFePO<sub>4</sub> was charged at 10 mA g<sup>-1</sup> up to 0.6 V vs AC, respectively, in 1 M Ca(TFSI)<sub>2</sub> in acetonitrile using an AC anode at room temperature (acetonitrile was only used for Na<sup>+</sup>

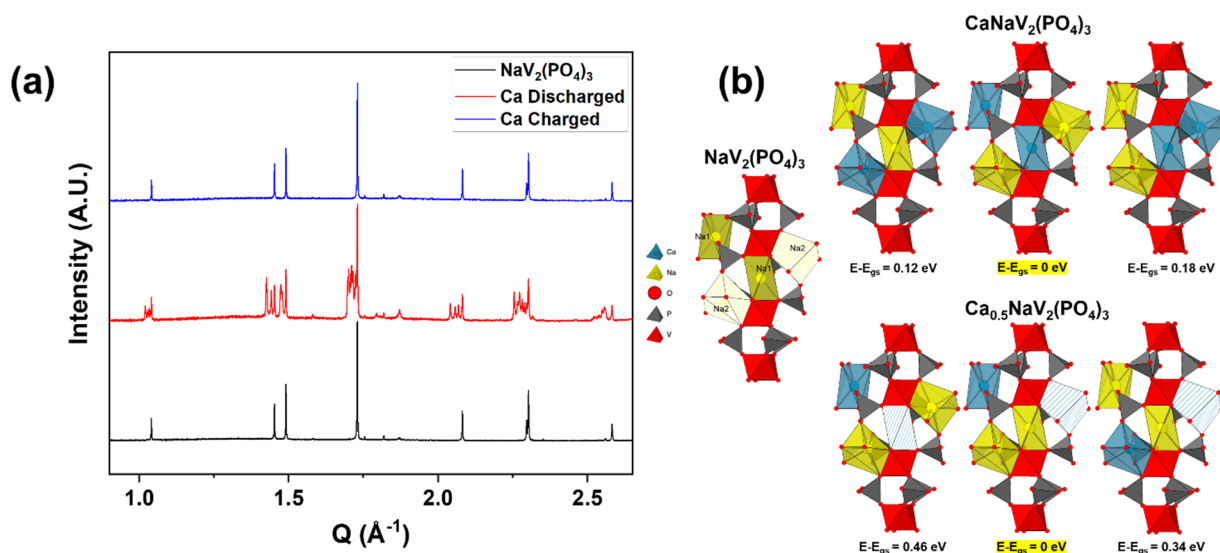


Figure 2. Ex situ synchrotron XRD patterns of (a)  $\text{NaV}_2(\text{PO}_4)_3$  and (b) DFT-optimized structures of  $\text{NaV}_2(\text{PO}_4)_3$ ,  $\text{CaNaV}_2(\text{PO}_4)_3$ , and  $\text{Ca}_{0.5}\text{NaV}_2(\text{PO}_4)_3$  with various Ca and Na sites.

and  $\text{Li}^+$  removal). After charging, the electrodes were washed with fresh acetonitrile to remove any residual salt on the surface. Diglyme was chosen as the electrolyte solvent for the Ca intercalation reactions because of its good thermal stability, high salt solubility, and large potential window.<sup>42,43</sup> As the effort is focused on identifying and evaluating cathode materials (and to avoid possible  $\text{CaF}_2$  passivation of a Ca metal anode), electrodes were tested against capacitive-type AC electrodes. The charging curve of  $\text{Na}_3\text{V}_2(\text{PO}_4)_3$  (Figure S1a) showed a voltage plateau around 0.1 V vs AC with a charge capacity of  $108 \text{ mA h g}^{-1}$  corresponding to 92% theoretical capacity based on the expected endmember,  $\text{NaV}_2(\text{PO}_4)_3$ .  $\text{LiFePO}_4$  showed similar behavior (Figure S2a) with a voltage plateau around  $-0.06 \text{ V}$  vs AC and a charge capacity of  $159 \text{ mA h g}^{-1}$  corresponding to 93.5% of theoretical capacity, representing nearly complete  $\text{Li}^+$  extraction in the electrochemical window. These data confirm that the potential of the AC electrode utilized is stable and functions well as a quasireference electrode.

To confirm the structure and purity of each phase, synchrotron XRD studies were performed on the pristine materials ( $\text{Na}_3\text{V}_2(\text{PO}_4)_3$ ,  $\text{LiFePO}_4$ ) and the charged samples ( $\text{NaV}_2(\text{PO}_4)_3$ ,  $\text{FePO}_4$ ) (see Figures S1b,c and S2b,c). Refinement details are described in the Supporting Information, while the refined lattice parameters of  $\text{Na}_3\text{V}_2(\text{PO}_4)_3$  and  $\text{LiFePO}_4$  at different states of charge obtained from Rietveld refinement are shown in Table 1.

The synthesized  $\text{NaV}_2(\text{PO}_4)_3$  and  $\text{FePO}_4$  materials were investigated as Ca-ion intercalation hosts by galvanostatic discharge/charge studies at constant current densities of  $3.5 \text{ mA g}^{-1}$  ( $\text{NaV}_2(\text{PO}_4)_3$ ) and  $7.5 \text{ mA g}^{-1}$  ( $\text{FePO}_4$ ) in  $0.5 \text{ M Ca}(\text{TFSI})_2$  in diglyme using an AC anode at room temperature (Figure 1). The voltage calibration with respect to voltage vs  $\text{Ca}^{2+}/\text{Ca}$  is described in the experimental section in the Supporting Information. In Figure 1a, it is demonstrated that the  $\text{NaV}_2(\text{PO}_4)_3$  electrode in this electrochemical system exhibits highly reversible first discharge and charge capacities of 81 and  $79 \text{ mA h g}^{-1}$ , corresponding to 0.608 mol of  $\text{Ca}^{2+}/\text{NaV}_2(\text{PO}_4)_3$  (charge capacity basis). The discharge–charge curves of the  $\text{Ca}_x[\text{NaV}_2(\text{PO}_4)_3]$  electrode show a voltage plateau around 3.2 V vs  $\text{Ca}^{2+}/\text{Ca}$  consistent with Ca

intercalation and deintercalation. Based on the calibration studies, the observed reversible insertion reaction voltage is generally higher than that seen for other well-studied multivalent chemistry systems and confirms the promise of polyanion cathodes in Ca-ion systems (Table S1). The  $dQ/dV$  profile has redox peaks at 3.25 and 3.29 V vs  $\text{Ca}^{2+}/\text{Ca}$ , corresponding to a hysteresis of only 0.04 V. This value is the smallest we are aware of for CIB electrodes and represents one of the first multivalent-based energy storage systems with such highly reversible reaction kinetics and small interfacial problems.<sup>44,45</sup> In addition to the NASICON framework, the  $\text{FePO}_4$  olivine electrode was found to exhibit capacities of 103 and  $72 \text{ mA h g}^{-1}$  for the first discharge and charge, respectively, a 30% drop in reversible capacity on the first cycle. The differences in the materials that may cause such changes to be manifested will be discussed later in the discussion (Figure 1b). For the olivine, the charge capacity corresponds to 40.5% of the theoretical value (based on the mass of  $\text{FePO}_4$ ) or  $\sim 0.2 \text{ mol}$  of  $\text{Ca}^{2+}$  per  $\text{FePO}_4$ . The  $\text{FePO}_4$  electrodes also showed voltage plateaus near 2.9 V (vs  $\text{Ca}^{2+}/\text{Ca}$ ) in the discharge–charge curves, similar to the value seen in  $\text{Ca}_x[\text{NaV}_2(\text{PO}_4)_3]$  and consistent with the values expected for  $\text{Ca}^{2+}$  intercalation/deintercalation based on reported  $\text{Na}_x[\text{FePO}_4]$  studies.<sup>37</sup> The redox peak potentials in the  $dQ/dV$  curves are 3.04 and 3.15 V (vs  $\text{Ca}^{2+}/\text{Ca}$ ), with a hysteresis of 0.11 V.

The cycling performance of the  $\text{NaV}_2(\text{PO}_4)_3$  and  $\text{FePO}_4$  host electrodes was investigated at room temperature at constant current densities of  $3.5 \text{ mA g}^{-1}$  ( $\text{NaV}_2(\text{PO}_4)_3$ ) and  $7.5 \text{ mA g}^{-1}$  ( $\text{FePO}_4$ ). (Figure 1c,d) The  $\text{NaV}_2(\text{PO}_4)_3$  electrode delivered a reversible and relatively stable discharge capacity of  $83 \text{ mA h g}^{-1}$  after 40 cycles, indicating good capacity retention and a stable framework. In contrast,  $\text{FePO}_4$  showed significant capacity decay. Based on literature reports, the cycling performance of Mg-ion olivine cathodes in glyme electrolytes has been reported to also have higher capacity fade than expected probably due to either impedance increases or cation trapping side reactions associated with surface degradation reactions.<sup>46</sup>

As in many of these complex multivalent battery systems, several reported early studies were based on inadvertent

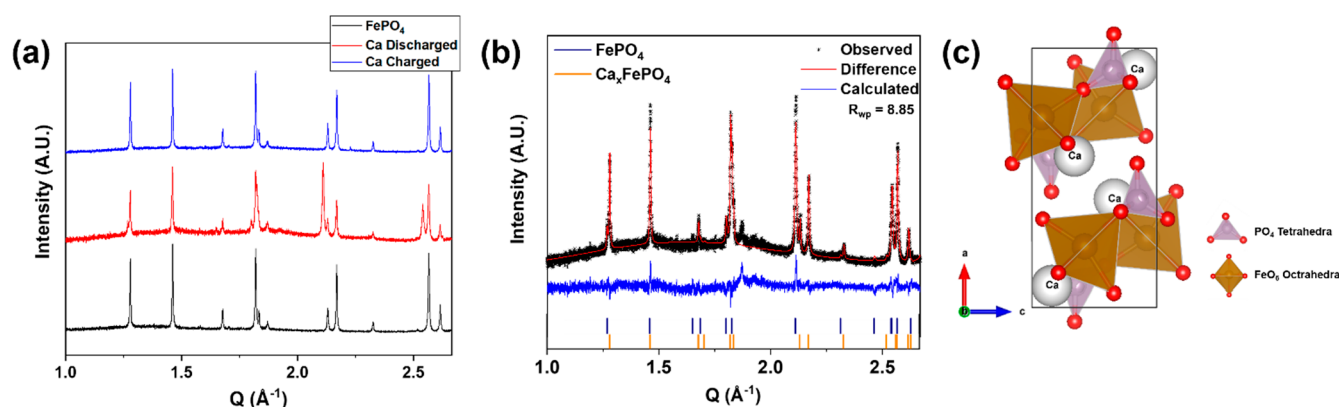


**Figure 3.** Ex situ synchrotron XRD patterns of (a)  $\text{FePO}_4$  at different states of charge. (b) High-resolution XRD data Rietveld refinement of calciated  $\text{FePO}_4$ . (c) Tentative Ca position in calciated  $\text{FePO}_4$  suggested by Rietveld refinement. Possible distortions of the framework are not shown.

mixtures of cations, proton involvement, or simply corrosion reactions mimicking the desired electrochemical activity. With this history and a paucity of Ca-specific spectroscopic detection techniques commonly available, e.g.,  $^{43}\text{Ca}$  MAS NMR, it is necessary to confirm the transporting species and their nature to gain insights into the energy storage mechanism involved. To ensure that  $\text{Ca}^{2+}$  intercalation is the predominant electrochemical reaction for  $\text{NaV}_2(\text{PO}_4)_3$  and  $\text{FePO}_4$  frameworks, ex situ synchrotron XRD data of discharged and charged electrodes was collected and studied. The diffraction patterns, shown in Figure 2, were normalized to the highest peak intensity of the active materials to compensate for particle size differences and materials processing artifacts. Reversible structural changes were observed for both  $\text{NaV}_2(\text{PO}_4)_3$  and  $\text{FePO}_4$  upon cycling consistent with changes in the diffraction pattern and lattice versus state of charge. In the diffraction pattern of discharged  $\text{NaV}_2(\text{PO}_4)_3$ , seen in Figure 2a (middle), a new set of diffraction peaks appears on the lower-angle side of each peak of the  $\text{NaV}_2(\text{PO}_4)_3$  phase, consistent with lattice expansion and intercalation of  $\text{Ca}^{2+}$ . Fully resolving these new larger unit cell phases was not possible due to the significant overlap of peaks belonging to these closely related multiple phases. A possible monoclinic distortion upon reduction, as noted in the fully sodiated phase  $\text{Na}_3\text{V}_2(\text{PO}_4)_3$ , increased the difficulty of a definitive phase identification from the data. The formation of a complex mixture of related new phases is consistent with isolation of various metastable phases in the system derived from partial vacancy/ $\text{Ca}^{2+}$  ordering due to slow  $\text{Ca}^{2+}$  diffusion<sup>23,47</sup> or possibly  $\text{Na}^+/\text{Ca}^{2+}$  reordering.<sup>41,48</sup> Although not evaluated fully to date, the use of longer equilibration times, voltage holds, or higher temperatures may resolve some of the structural issues associated with these metastable phases. Its implication on the Ca-ion insertion mechanism will be discussed after the data from the XAS studies is presented. DFT (density functional theory) calculations were performed (Figure 2b) on both  $\text{CaNaV}_2(\text{PO}_4)_3$  and  $\text{Ca}_{0.5}\text{NaV}_2(\text{PO}_4)_3$  in order to evaluate the cation diffusion pathway. The study indicated that the most energetically favorable state involved some cation mixing over the two possible crystallographic sites (6b, 18e). Although consistent with previous NASICON cation diffusion pathway studies, our diffraction data was not of sufficient resolution to investigate this model.<sup>41,50</sup> Notably, after charging ( $\text{Ca}^{2+}$  removal) the  $\text{Ca}_x[\text{NaV}_2(\text{PO}_4)_3]$  reduced phase, the XRD pattern of the initial charged  $\text{NaV}_2(\text{PO}_4)_3$  phase is regenerated,

demonstrating the high reversibility of  $\text{Ca}^{2+}$  intercalation/deintercalation in the NASICON structure (Figures 2a and S4a and Table 1). This assessment is consistent with the high-resolution XRD data in Figure 2a that shows that small differences in Na/Ca stoichiometry or ordering are manifested as detectable changes in the patterns.

In contrast to the  $\text{NaV}_2(\text{PO}_4)_3$  NASICON studies, for  $\text{FePO}_4$ , only a single new orthorhombic phase was detected by high-resolution XRD when the cathode was discharged in a Ca-ion electrolyte (Figure 3a). Both  $\text{FePO}_4$  and a calciated  $\text{FePO}_4$  phase were studied and compared using the diffraction data collected (Figure 3b). The initial refinements in space group  $Pnma$  suggested that  $\text{Ca}^{2+}$  ions were not occupying the Li site (from  $\text{LiFePO}_4$ ) nor the crystallographic site ( $Pnma$  space group) identified in the sodium analogue ( $\text{NaFePO}_4$ ).<sup>37</sup> As calcium cations are commonly observed in an oxide coordination greater than six and as suggested by the Fourier map (see Supporting Information), the  $\text{Ca}^{2+}$  cation may prefer to occupy a site near (but not on) the original Li site (Figure 3c), unlike the Na analogue.<sup>37</sup> However, due to poor peak intensity at high angles and significant overlapping peaks, the true location and fraction of the  $\text{Ca}^{2+}$  cation could not be refined with confidence. Rietveld refinement indicated mixed phases consistent with a weight ratio of  $\text{FePO}_4$  to the calciated  $\text{FePO}_4$  phase of approximately 55 to 45%. After charging, the  $\text{FePO}_4$  phase is completely recovered with similar peak widths to the initial diffraction pattern, indicating the good reversibility of Ca intercalation and deintercalation into the olivine structure (Figures 3a and S4b and Table 1). The diffraction and electrochemical evidence together suggest that the large ( $\sim 30\%$ ) irreversible capacity shown in the first cycle probably does not arise from an incomplete charging reaction, e.g., electronic isolation of a  $\text{Ca}_x[\text{FePO}_4]$  phase, but probably from electrolyte-based side reactions that are associated with surface degradation reactions that consume active  $\text{Ca}^{2+}$  that is thus unavailable to future cycles, similar to passivation layers in LIBs that trap lithium cations and contribute to poor Coulombic efficiency.

XAS was used to study changes in the local structure of the transition metal species (i.e., the transition metal V, Fe sites) and verify changes in their oxidation state in response to calcium intercalation and deintercalation. Figure 4a,b show the V K-edge and Fe K-edge X-ray absorption near-edge structure (XANES) spectra of  $\text{NaV}_2(\text{PO}_4)_3$  and  $\text{FePO}_4$ , respectively, at different charge states during cycling. To first order, XANES



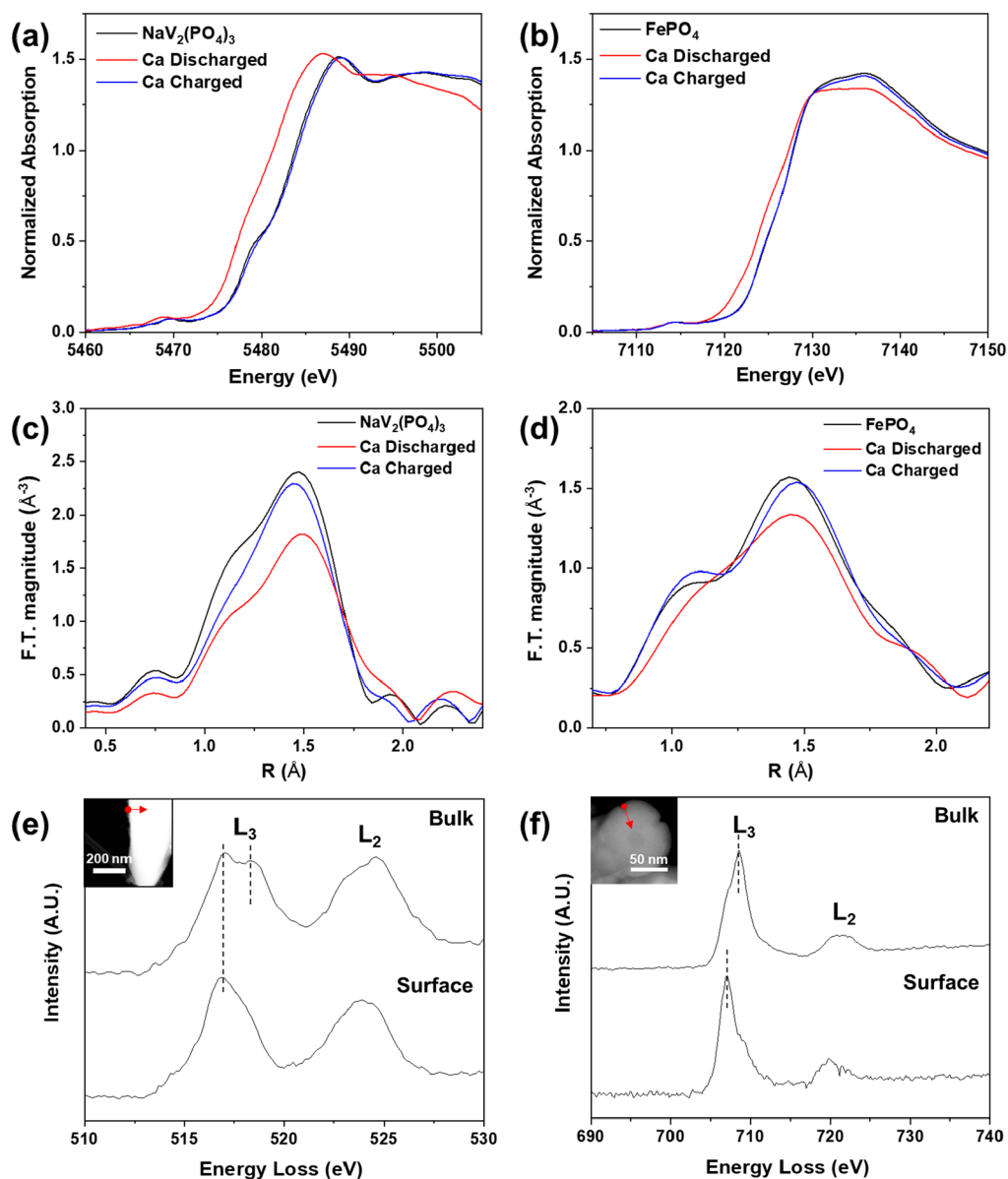


Figure 4. Ex situ (a) V K-edge XANES spectra of  $\text{NaV}_2(\text{PO}_4)_3$  and (b) Fe K-edge XANES spectra of  $\text{FePO}_4$  at different states of charge. Ex situ (c) V K-edge EXAFS spectra of  $\text{NaV}_2(\text{PO}_4)_3$  and (d) Fe K-edge EXAFS spectra of  $\text{FePO}_4$  at different states of charge (phase is not corrected). EELS spectra of (e) calcinated  $\text{NaV}_2(\text{PO}_4)_3$  and (f) calcinated  $\text{FePO}_4$ . The insets show the EELS acquisition area indicating the direction from the surface to bulk. Ten nm from the edge of the particle is considered as a threshold for the surface and bulk.

data provide a bulk-averaged measure of the transition metal oxidation state and has been commonly used to study charge transfer in both Li-ion and multivalent battery chemistries.<sup>49–51</sup> The position of the main edge, corresponding to a  $1s \rightarrow 4p$  transition, is affected by the degree of screening of the transition metal valence electrons.<sup>52,53</sup> When the  $\text{NaV}_2(\text{PO}_4)_3$  electrode was discharged, the V K-edge shifted approximately 2.5 eV toward lower energies due to the reduction of  $\text{V}^{4+}$  toward  $\text{V}^{3+}$  (Figure 4a). After charging, the V K-edge shifted back to the original position of  $\text{NaV}_2(\text{PO}_4)_3$ , consistent with oxidation to  $\text{V}^{4+}$ . The  $\text{FePO}_4$  electrodes showed a similar tendency (Figure 4b). A reversible Fe K-edge shift was observed during cycling, indicating the reversible oxidation state change of Fe. However, the Fe K-edge had less of a relative shift than the V K-edge, consistent with less calcium insertion seen in the electrochemical and diffraction-based experiments. This agrees with the relative active material

utilizations, where  $\text{NaV}_2(\text{PO}_4)_3$  and  $\text{FePO}_4$  delivered 60.5 and 40.5% theoretical capacities, respectively.

The local environment around the transition metal atom (V, Fe) was also investigated using extended X-ray absorption fine structure (EXAFS) spectra at different states of charge (Figure 4c,d). The first peak in the Fourier-transformed EXAFS data is due to scattering from the nearest neighbor oxygen atoms. The amplitude of this peak decreased for both  $\text{NaV}_2(\text{PO}_4)_3$  and  $\text{FePO}_4$ , suggesting the  $\text{VO}_6$  and  $\text{FeO}_6$  octahedral distortion upon calcination. After charging, the amplitude was recovered, indicating good reversibility of the local structure.

The valence states of the transition metals were studied by EELS, providing similar electronic structure information to XAS but with atomic-scale spatial resolution. EELS was measured from the surface and bulk region of calcinated  $\text{NaV}_2(\text{PO}_4)_3$  and  $\text{FePO}_4$ . Figure 4e,f show the  $L_{2,3}$ -edges of the transition metals (V, Fe) originating from the excitation of 2p

electrons to the unoccupied 3d states of the metals. The calciated  $\text{NaV}_2(\text{PO}_4)_3$  showed the V  $L_3$ -edge peak at 517 eV from the surface, which is the characteristic peak of  $\text{V}^{3+}$ .<sup>54,55</sup> On the other hand, two V  $L_3$ -edge peaks from the bulk were observed at 517 and 518.35 eV, indicating the bulk region consists of both  $\text{V}^{3+}$  and  $\text{V}^{4+}$  considering the high-energy peak represents a higher oxidation state.<sup>55</sup> The calciated  $\text{FePO}_4$  showed a similar trend. The Fe  $L_3$ -edge from the surface showed a peak at 707.05 eV, and the Fe  $L_3$ -edge from the bulk shifted to higher energy by  $\sim 1.5$  eV compared to the surface, indicating that the oxidation state of Fe at the surface is 2+, while  $\text{Fe}^{3+}$  is dominant in the bulk.<sup>56</sup> In summary, the reduced valence states of transition metals due to calciation were confirmed by EELS, but the oxidation state was not found to be uniform starting from the surface and moving to the bulk (core). Because both XAS and XRD studies indicate that  $\text{Ca}^{2+}$  intercalation did not occur uniformly across the active materials and both types of materials tested below theoretical capacity under the conditions used in this study, the working model postulated for these partially calciated discharged products is an active particle with a calcium-rich surface relative to the bulk composition. Further materials optimization studies, including nanoscale synthesis of the cathodes to give a shorter Ca diffusion length and using a higher-temperature cell testing protocol to increase the diffusion rate, may increase the uniformity of the particle and unite the surface and bulk compositions. In preliminary testing, cycling the  $\text{FePO}_4$  electrode in Ca-ion electrolytes at 50 °C did show a higher specific capacity (Figure S5) and will be investigated in future efforts.

To track the calcium ions in the system, EDS studies were carried out to quantify the amount of Ca insertion and extraction during cycling (Figure 5a,b). Using  $\text{NaV}_2(\text{PO}_4)_3$  and  $\text{FePO}_4$  electrodes that were washed thoroughly with acetonitrile to ensure that no calcium electrolyte salt residue remained on the surface (experimentally, no electrolyte components, notably the sulfur atom from the salt TFSI<sup>-</sup> anion, were detected). EDS spectra were normalized to the transition metal signal (V, Fe). The  $\text{NaV}_2(\text{PO}_4)_3$  electrode showed distinct Ca signals at 3.7 keV for Ca  $K\alpha$  and 4.0 keV for Ca  $K\beta$  after discharge. After charging, the Ca signal was significantly diminished relative to the metals, indicating Ca deintercalation. The  $\text{FePO}_4$  electrode showed similar behavior but with more residual Ca in the spectra relative to the metals in the framework, probably related to the higher first cycle irreversible capacity losses (Figure S4b and Table 1). The amount of Ca in  $\text{NaV}_2(\text{PO}_4)_3$  and  $\text{FePO}_4$  electrodes based on the EDS quantification results and calculated from the discharge and charge capacity of EDS samples is shown in Figure 5c and is in rough agreement with the values determined from the electrochemical studies. Mechanistically, an important outcome of the EDS study besides confirmation of calcium cycling was that the Na content did not change significantly during the electrochemical cycling, including a comparison of a Ca-ion electrolyte cycled  $\text{NaV}_2(\text{PO}_4)_3$  and the uncycled  $\text{NaV}_2(\text{PO}_4)_3$ . This is consistent with Ca ions being the active transporting species and the sodium, under the testing conditions used, being electrochemically inaccessible. This trapping of sodium is also consistent with synthesis of the simple  $\text{V}_2(\text{PO}_4)_3$  NASICON framework, which cannot be isolated from  $\text{Na}_3\text{V}_2(\text{PO}_4)_3$  (it can only be prepared chemically starting from the lithium analogue, using an  $\text{NO}_2\text{BF}_4/\text{AN}$  solution under nitrogen<sup>57</sup>). We expect some discrepancy in the

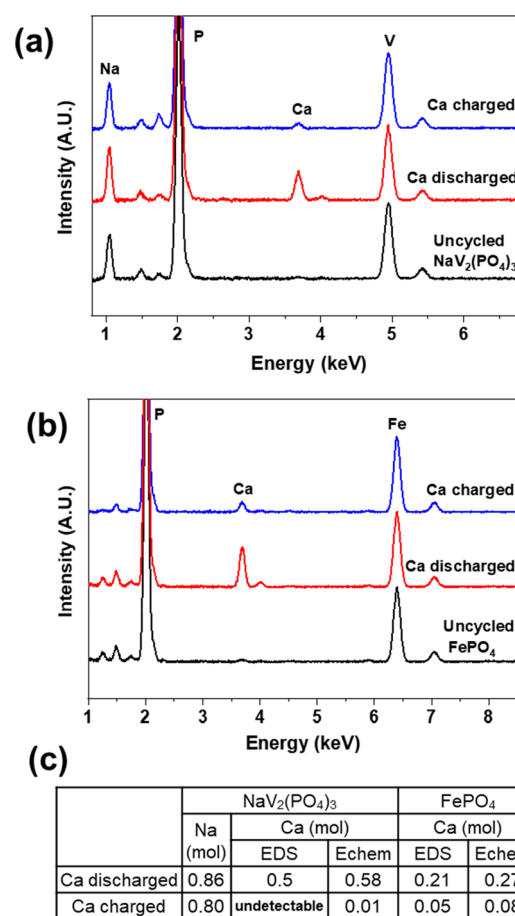


**Figure 5.** Ex situ EDS spectra of (a)  $\text{NaV}_2(\text{PO}_4)_3$  and (b)  $\text{FePO}_4$  before cycling and after discharge and charge in Ca cells. (c) EDS results for  $\text{NaV}_2(\text{PO}_4)_3$  and  $\text{FePO}_4$ .

EDS results is due to different sample and measurement conditions and the complexity of the sample containing a large amount of carbon, binder, and current collector. Nonetheless, the data clearly show that reversible Ca intercalation in both  $\text{NaV}_2(\text{PO}_4)_3$  and  $\text{FePO}_4$  occurs, which is consistent with the evidence from the other complementary characterization methods.

In conclusion, we report on two polyanionic phosphates, the NASICON-type  $\text{NaV}_2(\text{PO}_4)_3$  and the olivine-type  $\text{FePO}_4$ , and they were studied as CIB cathodes at room temperature in a nonaqueous electrolyte for the first time. Both  $\text{NaV}_2(\text{PO}_4)_3$  and  $\text{FePO}_4$  can reversibly intercalate  $\text{Ca}^{2+}$  in a cell that uses a capacitive AC anode at a high voltage vs a  $\text{Ca}^{2+}/\text{Ca}$  glyme-based electrolyte. Based on synchrotron XRD, XAS, EELS, and EDS results, we have confirmed that Ca can be intercalated into and deintercalated from the sodium stabilized NASICON framework material  $\text{NaV}_2(\text{PO}_4)_3$  (0.6 mol of  $\text{Ca}^{2+}$ ) with stable cyclability for over 40 cycles. In contrast, the olivine material  $\text{FePO}_4$  (0.2 mol of  $\text{Ca}^{2+}$ ) cycles but suffers from capacity decay probably due to side reactions on the surface that consume active calcium ions in the electrolyte, which is consistent with the diffraction data that shows retention of framework integrity and crystallinity on cycling. The  $\text{NaV}_2(\text{PO}_4)_3$  cathode exhibited an initial discharge capacity of 81 mA h  $\text{g}^{-1}$  at 3.5 mA  $\text{g}^{-1}$  with a discharge plateau around 3.2 V vs  $\text{Ca}^{2+}/\text{Ca}$ . The  $\text{FePO}_4$  cathode showed an initial discharge capacity of 103 mA h  $\text{g}^{-1}$  at 7.5 mA  $\text{g}^{-1}$  at room temperature with a discharge

plateau around 2.9 V vs  $\text{Ca}^{2+}/\text{Ca}$ . Both  $\text{NaV}_2(\text{PO}_4)_3$  and  $\text{FePO}_4$  showed well-defined voltage plateaus and a small voltage hysteresis ( $\text{NaV}_2(\text{PO}_4)_3$ : 0.04 V,  $\text{FePO}_4$ : 0.11 V), making the NASICON, notably, a possible candidate for future CIB full cell development as the next generation of anode materials is developed. Future studies will identify conditions to further improve cyclability. We also report that both  $\text{NaV}_2(\text{PO}_4)_3$  and  $\text{FePO}_4$  lattices insert calcium ions using different Ca intercalation mechanisms compared to either of their Na and Li analogues and demonstrate good structural stability during  $\text{Ca}^{2+}$  intercalation and deintercalation. We believe that this work demonstrates that polyanion phosphates are promising host candidates for CIBs and will spur further research on polyanionic phosphates as electrode materials for CIBs.

## ■ ASSOCIATED CONTENT

### SI Supporting Information

The Supporting Information is available free of charge at <https://pubs.acs.org/doi/10.1021/acsenergylett.0c01663>.

Experimental methods and additional figures and tables: electrochemical data, XRD patterns, and Rietveld refinement of ex situ samples, crystal structure, magnified XRD patterns, electrochemical data at elevated temperature, SEM, voltage calibration, voltage comparison with other multivalent chemistry systems, and refined parameters of ex situ samples (PDF)

## ■ AUTHOR INFORMATION

### Corresponding Authors

**John T. Vaughey** – Chemical Sciences and Engineering Division and Joint Center for Energy Storage Research, Argonne National Laboratory, Lemont, Illinois 60439, United States; [orcid.org/0000-0002-2556-6129](https://orcid.org/0000-0002-2556-6129); Email: [vaughey@anl.gov](mailto:vaughey@anl.gov)

**Linda F. Nazar** – Joint Center for Energy Storage Research, Argonne National Laboratory, Lemont, Illinois 60439, United States; Department of Chemistry and the Waterloo Institute for Nanotechnology, University of Waterloo, Waterloo, Ontario N2L 3G1, Canada; [orcid.org/0000-0002-3314-8197](https://orcid.org/0000-0002-3314-8197); Email: [lnazar@uwaterloo.ca](mailto:lnazar@uwaterloo.ca)

### Authors

**Sanghyeon Kim** – Chemical Sciences and Engineering Division and Joint Center for Energy Storage Research, Argonne National Laboratory, Lemont, Illinois 60439, United States; [orcid.org/0000-0003-2789-449X](https://orcid.org/0000-0003-2789-449X)

**Liang Yin** – Joint Center for Energy Storage Research and X-ray Science Division, Advanced Photon Source, Argonne National Laboratory, Lemont, Illinois 60439, United States; [orcid.org/0000-0001-5396-782X](https://orcid.org/0000-0001-5396-782X)

**Myeong Hwan Lee** – Department of Materials Science and Engineering, Research Institute of Advanced Materials (RIAM), Seoul National University, Seoul 08826, Republic of Korea

**Prakash Parajuli** – Joint Center for Energy Storage Research, Argonne National Laboratory, Lemont, Illinois 60439, United States; Department of Physics, University of Illinois at Chicago, Chicago, Illinois 60607, United States

**Lauren Blanc** – Joint Center for Energy Storage Research, Argonne National Laboratory, Lemont, Illinois 60439, United States; Department of Chemistry and the Waterloo Institute for

Nanotechnology, University of Waterloo, Waterloo, Ontario N2L 3G1, Canada

**Timothy T. Fister** – Chemical Sciences and Engineering Division and Joint Center for Energy Storage Research, Argonne National Laboratory, Lemont, Illinois 60439, United States; [orcid.org/0000-0001-6537-6170](https://orcid.org/0000-0001-6537-6170)

**Haesun Park** – Joint Center for Energy Storage Research and Materials Science Division, Argonne National Laboratory, Lemont, Illinois 60439, United States; [orcid.org/0000-0001-6266-8151](https://orcid.org/0000-0001-6266-8151)

**Bob Jin Kwon** – Chemical Sciences and Engineering Division and Joint Center for Energy Storage Research, Argonne National Laboratory, Lemont, Illinois 60439, United States; [orcid.org/0000-0001-7395-0814](https://orcid.org/0000-0001-7395-0814)

**Brian J. Ingram** – Chemical Sciences and Engineering Division and Joint Center for Energy Storage Research, Argonne National Laboratory, Lemont, Illinois 60439, United States

**Peter Zapol** – Joint Center for Energy Storage Research and Materials Science Division, Argonne National Laboratory, Lemont, Illinois 60439, United States; [orcid.org/0000-0003-0570-9169](https://orcid.org/0000-0003-0570-9169)

**Robert F. Klie** – Joint Center for Energy Storage Research, Argonne National Laboratory, Lemont, Illinois 60439, United States; Department of Physics, University of Illinois at Chicago, Chicago, Illinois 60607, United States; [orcid.org/0000-0003-4773-6667](https://orcid.org/0000-0003-4773-6667)

**Kisuk Kang** – Center for Nanoparticle Research, Institute for Basic Science (IBS), Institute of Engineering Research, College of Engineering, and Department of Materials Science and Engineering, Research Institute of Advanced Materials (RIAM), Seoul National University, Seoul 08826, Republic of Korea; [orcid.org/0000-0002-8696-1886](https://orcid.org/0000-0002-8696-1886)

**Saul H. Lapidus** – Joint Center for Energy Storage Research and X-ray Science Division, Advanced Photon Source, Argonne National Laboratory, Lemont, Illinois 60439, United States; [orcid.org/0000-0002-7486-4325](https://orcid.org/0000-0002-7486-4325)

Complete contact information is available at: <https://pubs.acs.org/doi/10.1021/acsenergylett.0c01663>

### Notes

The authors declare no competing financial interest.

## ■ ACKNOWLEDGMENTS

This work was supported by the Joint Center for Energy Storage Research, an Energy Innovation Hub funded by the U.S. Department of Energy, Office of Science, Basic Energy Sciences. This research used resources of the Advanced Photon Source, a U.S. Department of Energy (DOE) Office of Science User Facility operated for the DOE Office of Science by Argonne National Laboratory under Contract No. DE-AC02-06CH11357. This work is conducted at Argonne National Laboratory supported by the U.S. Department of Energy under contract DE-A02-06CH11357. The acquisition of JEOL JEM ARM200CF at the University of Illinois at Chicago was supported by an MRI-R2 grant from the National Science Foundation (Grant No. DMR-0959470), and the upgraded Gatan Continuum spectrometer was supported by a grant from the NSF (DMR-1626065).



## REFERENCES

- (1) Etacheri, V.; Marom, R.; Elazari, R.; Salitra, G.; Aurbach, D. Challenges in the development of advanced Li-ion batteries: a review. *Energy Environ. Sci.* **2011**, *4*, 3243–3262.
- (2) Blomgren, G. E. The Development and Future of Lithium Ion Batteries. *J. Electrochem. Soc.* **2017**, *164*, A5019–A5025.
- (3) Ponrouch, A.; Bitenc, J.; Dominko, R.; Lindahl, N.; Johansson, P.; Palacin, M. R. Multivalent rechargeable batteries. *Energy Storage Mater.* **2019**, *20*, 253–262.
- (4) Liu, M.; Rong, Z.; Malik, R.; Canepa, P.; Jain, A.; Ceder, G.; Persson, K. A. Spinel compounds as multivalent battery cathodes: a systematic evaluation based on ab initio calculations. *Energy Environ. Sci.* **2015**, *8*, 964–974.
- (5) Canepa, P.; Sai Gautam, G.; Hannah, D. C.; Malik, R.; Liu, M.; Gallagher, K. G.; Persson, K. A.; Ceder, G. Odyssey of Multivalent Cathode Materials: Open Questions and Future Challenges. *Chem. Rev.* **2017**, *117*, 4287–4341.
- (6) Ponrouch, A.; Palacin, M. R. On the road toward calcium-based batteries. *Curr. Opin. Electrochem.* **2018**, *9*, 1–7.
- (7) Gummow, R. J.; Vamvounis, G.; Kannan, M. B.; He, Y. Calcium-Ion Batteries: Current State-of-the-Art and Future Perspectives. *Adv. Mater.* **2018**, *30*, No. 1801702.
- (8) Ponrouch, A.; Frontera, C.; Barde, F.; Palacin, M. R. Towards a calcium-based rechargeable battery. *Nat. Mater.* **2016**, *15*, 169–72.
- (9) Wang, D.; Gao, X.; Chen, Y.; Jin, L.; Kuss, C.; Bruce, P. G. Plating and stripping calcium in an organic electrolyte. *Nat. Mater.* **2018**, *17*, 16–20.
- (10) Li, Z.; Fuhr, O.; Fichtner, M.; Zhao-Karger, Z. Towards stable and efficient electrolytes for room-temperature rechargeable calcium batteries. *Energy Environ. Sci.* **2019**, *12*, 3496–3501.
- (11) Ta, K.; Zhang, R.; Shin, M.; Rooney, R. T.; Neumann, E. K.; Gewirth, A. A. Understanding Ca Electrodeposition and Speciation Processes in Nonaqueous Electrolytes for Next-Generation Ca-Ion Batteries. *ACS Appl. Mater. Interfaces* **2019**, *11*, 21536–21542.
- (12) Shyamsunder, A.; Blanc, L. E.; Assoud, A.; Nazar, L. F. Reversible Calcium Plating and Stripping at Room Temperature Using a Borate Salt. *ACS Energy Lett.* **2019**, *4*, 2271–2276.
- (13) Park, J.; Xu, Z. L.; Yoon, G.; Park, S. K.; Wang, J.; Hyun, H.; Park, H.; Lim, J.; Ko, Y. J.; Yun, Y. S.; Kang, K. Stable and High-Power Calcium-Ion Batteries Enabled by Calcium Intercalation into Graphite. *Adv. Mater.* **2020**, *32*, No. 1904411.
- (14) Richard Prabakar, S. J.; Ikhe, A. B.; Park, W. B.; Chung, K. C.; Park, H.; Kim, K. J.; Ahn, D.; Kwak, J. S.; Sohn, K. S.; Pyo, M. Graphite as a Long-Life  $\text{Ca}^{2+}$ -Intercalation Anode and its Implementation for Rocking-Chair Type Calcium-Ion Batteries. *Adv. Sci.* **2019**, *6*, 1902129.
- (15) Wang, M.; Jiang, C.; Zhang, S.; Song, X.; Tang, Y.; Cheng, H. M. Reversible calcium alloying enables a practical room-temperature rechargeable calcium-ion battery with a high discharge voltage. *Nat. Chem.* **2018**, *10*, 667–672.
- (16) Lipson, A. L.; Pan, B.; Lapidus, S. H.; Liao, C.; Vaughey, J. T.; Ingram, B. J. Rechargeable Ca-Ion Batteries: A New Energy Storage System. *Chem. Mater.* **2015**, *27*, 8442–8447.
- (17) Tojo, T.; Sugiura, Y.; Inada, R.; Sakurai, Y. Reversible Calcium Ion Batteries Using a Dehydrated Prussian Blue Analogue Cathode. *Electrochim. Acta* **2016**, *207*, 22–27.
- (18) Adil, M.; Dutta, P. K.; Mitra, S. An Aqueous Ca-ion Full Cell Comprising BaHCF Cathode and MCMB Anode. *Chem. Select.* **2018**, *3*, 3687–3690.
- (19) Adil, M.; Sarkar, A.; Roy, A.; Panda, M. R.; Nagendra, A.; Mitra, S. Practical Aqueous Calcium-Ion Battery Full-Cells for Future Stationary Storage. *ACS Appl. Mater. Interfaces* **2020**, *12*, 11489–11503.
- (20) Vo, T. N.; Hur, J.; Kim, I. T. Enabling High Performance Calcium-Ion Batteries from Prussian Blue and Metal–Organic Compound Materials. *ACS Sustainable Chem. Eng.* **2020**, *8*, 2596–2601.
- (21) Wang, J.; Tan, S.; Xiong, F.; Yu, R.; Wu, P.; Cui, L.; An, Q.  $\text{VOPO}_4 \cdot 2\text{H}_2\text{O}$  as a new cathode material for rechargeable Ca-ion batteries. *Chem. Commun.* **2020**, *56*, 3805–3808.
- (22) Xu, X.; Duan, M.; Yue, Y.; Li, Q.; Zhang, X.; Wu, L.; Wu, P.; Song, B.; Mai, L. Bilayered  $\text{Mg}_{0.25}\text{V}_2\text{O}_5 \cdot \text{H}_2\text{O}$  as a Stable Cathode for Rechargeable Ca-Ion Batteries. *ACS Energy Lett.* **2019**, *4*, 1328–1335.
- (23) Cabello, M.; Nacimiento, F.; Alcántara, R.; Lavela, P.; Pérez Vicente, C.; Tirado, J. L. Applicability of Molybdate as an Electrode Material in Calcium Batteries: A Structural Study of Layer-type  $\text{Ca}_x\text{MoO}_3$ . *Chem. Mater.* **2018**, *30*, 5853–5861.
- (24) Tojo, T.; Tawa, H.; Oshida, N.; Inada, R.; Sakurai, Y. Electrochemical characterization of a layered  $\alpha\text{-MoO}_3$  as a new cathode material for calcium ion batteries. *J. Electroanal. Chem.* **2018**, *825*, 51–56.
- (25) Hayashi, M.; Arai, H.; Ohtsuka, H.; Sakurai, Y. Electrochemical insertion/extraction of calcium ions using crystalline vanadium oxide. *Electrochem. Solid-State Lett.* **2004**, *7*, A119.
- (26) Cabello, M.; Nacimiento, F.; González, J. R.; Ortiz, G.; Alcántara, R.; Lavela, P.; Pérez-Vicente, C.; Tirado, J. L. Advancing towards a veritable calcium-ion battery:  $\text{CaCo}_2\text{O}_4$  positive electrode material. *Electrochem. Commun.* **2016**, *67*, 59–64.
- (27) Hurlbutt, K.; Wheeler, S.; Capone, I.; Pasta, M. Prussian Blue Analogs as Battery Materials. *Joule* **2018**, *2*, 1950–1960.
- (28) Rong, Z.; Malik, R.; Canepa, P.; Sai Gautam, G.; Liu, M.; Jain, A.; Persson, K.; Ceder, G. Materials Design Rules for Multivalent Ion Mobility in Intercalation Structures. *Chem. Mater.* **2015**, *27*, 6016–6021.
- (29) Masquelier, C.; Croguennec, L. Polyanionic (phosphates, silicates, sulfates) frameworks as electrode materials for rechargeable Li (or Na) batteries. *Chem. Rev.* **2013**, *113*, 6552–6591.
- (30) Ni, Q.; Bai, Y.; Wu, F.; Wu, C. Polyanion-Type Electrode Materials for Sodium-Ion Batteries. *Adv. Sci.* **2017**, *4*, 1600275.
- (31) Gong, Z.; Yang, Y. Recent advances in the research of polyanion-type cathode materials for Li-ion batteries. *Energy Environ. Sci.* **2011**, *4*, 3223–3242.
- (32) Huang, Z.-D.; Masese, T.; Orikasa, Y.; Mori, T.; Yamamoto, K. Vanadium phosphate as a promising high-voltage magnesium ion (de)-intercalation cathode host. *RSC Adv.* **2015**, *5*, 8598–8603.
- (33) Rubio, S.; Liu, R.; Liu, X.; Lavela, P.; Tirado, J. L.; Li, Q.; Liang, Z.; Ortiz, G. F.; Yang, Y. Exploring the high-voltage  $\text{Mg}^{2+}/\text{Na}^+$  co-intercalation reaction of  $\text{Na}_3\text{VCr}(\text{PO}_4)_3$  in Mg-ion batteries. *J. Mater. Chem. A* **2019**, *7*, 18081–18091.
- (34) Shan, P.; Gu, Y.; Yang, L.; Liu, T.; Zheng, J.; Pan, F. Olivine  $\text{FePO}_4$  Cathode Material for Rechargeable Mg-Ion Batteries. *Inorg. Chem.* **2017**, *56*, 13411–13416.
- (35) Zeng, J.; Yang, Y.; Lai, S.; Huang, J.; Zhang, Y.; Wang, J.; Zhao, J. A Promising High-Voltage Cathode Material Based on Mesoporous  $\text{Na}_3\text{V}_2(\text{PO}_4)_3/\text{C}$  for Rechargeable Magnesium Batteries. *Chem. - Eur. J.* **2017**, *23*, 16898–16905.
- (36) Nacimiento, F.; Cabello, M.; Alcántara, R.; Lavela, P.; Tirado, J. L. NASICON-type  $\text{Na}_3\text{V}_2(\text{PO}_4)_3$  as a new positive electrode material for rechargeable aluminium battery. *Electrochim. Acta* **2018**, *260*, 798–804.
- (37) Moreau, P.; Guyomard, D.; Gaubicher, J.; Boucher, F. Structure and Stability of Sodium Intercalated Phases in Olivine  $\text{FePO}_4$ . *Chem. Mater.* **2010**, *22*, 4126–4128.
- (38) Zeng, J.; Wu, D.; Wang, X.; Wu, J.; Li, J.; Wang, J.; Zhao, J. Insights into the Mg storage property and mechanism based on the honeycomb-like structured  $\text{Na}_3\text{V}_2(\text{PO}_4)_3/\text{C}/\text{G}$  in anhydrous electrolyte. *Chem. Eng. J.* **2019**, *372*, 37–45.
- (39) Aragón, M. J.; Lavela, P.; Recio, P.; Alcántara, R.; Tirado, J. L. On the influence of particle morphology to provide high performing chemically desodiated  $\text{C}@ \text{NaV}_2(\text{PO}_4)_3$  as cathode for rechargeable magnesium batteries. *J. Electroanal. Chem.* **2018**, *827*, 128–136.
- (40) Li, G.; Yang, Z.; Jiang, Y.; Jin, C.; Huang, W.; Ding, X.; Huang, Y. Towards polyvalent ion batteries: A zinc-ion battery based on NASICON structured  $\text{Na}_3\text{V}_2(\text{PO}_4)_3$ . *Nano Energy* **2016**, *25*, 211–217.



(41) Ko, J. S.; Paul, P. P.; Wan, G.; Seitzman, N.; DeBlock, R. H.; Dunn, B. S.; Toney, M. F.; Nelson Weker, J. NASICON  $\text{Na}_3\text{V}_2(\text{PO}_4)_3$  Enables Quasi-Two-Stage  $\text{Na}^+$  and  $\text{Zn}^{2+}$  Intercalation for Multivalent Zinc Batteries. *Chem. Mater.* **2020**, *32*, 3028–3035.

(42) Ha, S. Y.; Lee, Y. W.; Woo, S. W.; Koo, B.; Kim, J. S.; Cho, J.; Lee, K. T.; Choi, N. S. Magnesium(II) bis(trifluoromethane sulfonyl) imide-based electrolytes with wide electrochemical windows for rechargeable magnesium batteries. *ACS Appl. Mater. Interfaces* **2014**, *6*, 4063–4073.

(43) Shao, Y.; Liu, T.; Li, G.; Gu, M.; Nie, Z.; Engelhard, M.; Xiao, J.; Lv, D.; Wang, C.; Zhang, J. G.; Liu, J. Coordination chemistry in magnesium battery electrolytes: how ligands affect their performance. *Sci. Rep.* **2013**, *3*, 3130.

(44) Kwon, B. J.; Lau, K.-C.; Park, H.; Wu, Y. A.; Hawthorne, K. L.; Li, H.; Kim, S.; Bolotin, I. L.; Fister, T. T.; Zapol, P.; Klie, R. F.; Cabana, J.; Liao, C.; Lapidus, S. H.; Key, B.; Vaughey, J. T. Probing Electrochemical Mg-Ion Activity in  $\text{MgCr}_{2-x}\text{V}_x\text{O}_4$  Spinel Oxides. *Chem. Mater.* **2020**, *32*, 1162–1171.

(45) Tchitchekova, D. S.; Ponrouch, A.; Verrelli, R.; Broux, T.; Frontera, C.; Sorrentino, A.; Bardé, F.; Biskup, N.; Arroyo-de Dompablo, M. E.; Palacín, M. R. Electrochemical Intercalation of Calcium and Magnesium in  $\text{TiS}_2$ : Fundamental Studies Related to Multivalent Battery Applications. *Chem. Mater.* **2018**, *30*, 847–856.

(46) Zhang, R.; Ling, C. Unveil the Chemistry of Olivine  $\text{FePO}_4$  as Magnesium Battery Cathode. *ACS Appl. Mater. Interfaces* **2016**, *8*, 18018–18026.

(47) Hubaud, A. A.; Schroeder, D. J.; Key, B.; Ingram, B. J.; Dogan, F.; Vaughey, J. T. Low temperature stabilization of cubic  $(\text{Li}_{7-x}\text{Al}_{x/3})\text{-La}_3\text{Zr}_2\text{O}_{12}$ : role of aluminum during formation. *J. Mater. Chem. A* **2013**, *1*, 8813–8818.

(48) Wang, Q.; Zhang, M.; Zhou, C.; Chen, Y. Concerted Ion-Exchange Mechanism for Sodium Diffusion and Its Promotion in  $\text{Na}_3\text{V}_2(\text{PO}_4)_3$  Framework. *J. Phys. Chem. C* **2018**, *122*, 16649–16654.

(49) Lipson, A. L.; Kim, S.; Pan, B.; Liao, C.; Fister, T. T.; Ingram, B. J. Calcium intercalation into layered fluorinated sodium iron phosphate. *J. Power Sources* **2017**, *369*, 133–137.

(50) Yoo, H. D.; Jokisaari, J. R.; Yu, Y.-S.; Kwon, B. J.; Hu, L.; Kim, S.; Han, S.-D.; Lopez, M.; Lapidus, S. H.; Nolis, G. M.; et al. Intercalation of Magnesium into a Layered Vanadium Oxide with High Capacity. *ACS Energy Lett.* **2019**, *4*, 1528–1534.

(51) Bak, S. M.; Shadiké, Z.; Lin, R.; Yu, X.; Yang, X. Q. In Situ /Operando Synchrotron-Based X-Ray Techniques for Lithium-Ion Battery Research. *NPG Asia Mater.* **2018**, *10*, S63–S80.

(52) Horrocks, G. A.; Braham, E. J.; Liang, Y.; De Jesus, L. R.; Jude, J.; Velázquez, J. M.; Prendergast, D.; Banerjee, S. Vanadium K-Edge X-ray Absorption Spectroscopy as a Probe of the Heterogeneous Lithiation of  $\text{V}_2\text{O}_5$ : First-Principles Modeling and Principal Component Analysis. *J. Phys. Chem. C* **2016**, *120*, 23922–23932.

(53) Ali, G.; Lee, J. H.; Susanto, D.; Choi, S. W.; Cho, B. W.; Nam, K. W.; Chung, K. Y. Polythiophene-Wrapped Olivine  $\text{NaFePO}_4$  as a Cathode for Na-Ion Batteries. *ACS Appl. Mater. Interfaces* **2016**, *8*, 15422–15429.

(54) Gloter, A.; Serin, V.; Turquat, C.; Cesari, C.; Leroux, C.; Nihoul, G. Vanadium valency and hybridization in V-doped hafnia investigated by electron energy loss spectroscopy. *Eur. Phys. J. B* **2001**, *22*, 179–186.

(55) Yu, M.; Zeng, Y.; Han, Y.; Cheng, X.; Zhao, W.; Liang, C.; Tong, Y.; Tang, H.; Lu, X. Valence-Optimized Vanadium Oxide Supercapacitor Electrodes Exhibit Ultrahigh Capacitance and Super-Long Cyclic Durability of 100000 Cycles. *Adv. Funct. Mater.* **2015**, *25*, 3534–3540.

(56) Chueh, Y. L.; Lai, M. W.; Liang, J. Q.; Chou, L. J.; Wang, Z. L. Systematic Study of the Growth of Aligned Arrays of  $\alpha\text{-Fe}_2\text{O}_3$  and  $\text{Fe}_3\text{O}_4$  Nanowires by a Vapor–Solid Process. *Adv. Funct. Mater.* **2006**, *16*, 2243–2251.

(57) Park, M. J.; Yaghoobnejad Asl, H.; Therese, S.; Manthiram, A. Structural Impact of Zn-Insertion into Monoclinic  $\text{V}_2(\text{PO}_4)_3$ : Implications for Zn-Ion Batteries. *J. Mater. Chem. A* **2019**, *7*, 7159–7167.